

Provided for non-commercial research and education use.
Not for reproduction, distribution or commercial use.



(This is a sample cover image for this issue. The actual cover is not yet available at this time.)

This article appeared in a journal published by Elsevier. The attached copy is furnished to the author for internal non-commercial research and education use, including for instruction at the authors institution and sharing with colleagues.

Other uses, including reproduction and distribution, or selling or licensing copies, or posting to personal, institutional or third party websites are prohibited.

In most cases authors are permitted to post their version of the article (e.g. in Word or Tex form) to their personal website or institutional repository. Authors requiring further information regarding Elsevier's archiving and manuscript policies are encouraged to visit:

<http://www.elsevier.com/copyright>



Contents lists available at SciVerse ScienceDirect

Cold Regions Science and Technology

journal homepage: www.elsevier.com/locate/coldregions

Porosity of growing sea ice and potential for oil entrainment

Chris Petrich^{a,*}, Jonas Karlsson^b, Hajo Eicken^c^a Northern Research Institute, Narvik, Norway^b University of Copenhagen, Copenhagen, Denmark^c Geophysical Institute and International Arctic Research Center, University of Alaska Fairbanks, Fairbanks, AK, USA

ARTICLE INFO

Article history:

Received 6 June 2012

Accepted 16 December 2012

Available online 22 December 2012

Keywords:

Sea ice

Porosity

Oil

ABSTRACT

The pore space in the bottom-most layers of growing sea ice is directly connected to the ocean beneath, allowing for fluid exchange while providing a sheltered environment for sea-ice microbial communities. Because of its role as a habitat and its high porosity and permeability, potential entrainment of oil into this pore space is of broader concern. We estimate the ice volume that can potentially be infiltrated by oil and other buoyant pollutants in surface ocean water evaluating several years of sea ice measurements on undeformed landfast first-year sea ice at Barrow, Alaska. This ice is representative of undeformed sea ice in areas targeted for offshore oil development. The calculated ice volume is related to crude oil entrainment volumes with empirical relationships derived from field and laboratory measurements. We synthesize 12 years of sea-ice core salinity data and 6 years of quasi-continuous sea ice temperature profile measurements to derive the seasonal evolution of ice thickness and temperature gradients in sea ice. Porosity profiles are calculated from temperature and salinity profiles. Based on previous observations, an oil penetration depth is defined by a porosity threshold of 0.1 to 0.15. Ice thickness is found to increase from 0.6 m in January to its maximum of 1.5 m in May, and average temperature gradients at the ice–water interface range from $-15\text{ }^{\circ}\text{C}/\text{m}$ in January to $-2\text{ }^{\circ}\text{C}/\text{m}$ in May. Depending on ice temperature conditions, derived depths of fluid penetration range from 0.02 to 0.10 m in January to 0.12 to 0.25 m in May for a porosity threshold of 0.10. These penetration depths are approximately halved for a porosity threshold of 0.15. For average temperature conditions, expected entrainment of crude oil is less than $2\text{ L}/\text{m}^2$ in January and may be as high as 5 to $10\text{ L}/\text{m}^2$ in May. Accessible ice volume and entrainment potential are expected to increase during warm spells and with the opening of brine channel networks in late spring. Considering inhomogeneous spread and pooling of oil under ice, entrainment in warm sea ice is expected to add approximately 20% to previous estimates of the under-ice pooling capacity.

© 2012 Elsevier B.V. All rights reserved.

1. Introduction

Sea ice is a porous material that exchanges fluid with the underlying ocean during growth (e.g., Eide and Martin, 1975). This creates a small-scale marine environment that is both sheltered and connected to the ocean underneath. Thus, the bottom layers of sea ice are known to serve as a biological habitat (Cota and Smith, 1991; Gradinger et al., 2009; Krembs et al., 2000) but are also susceptible to entrainment and retention of oil spilled under the ice (e.g., Buist et al., 2008; Karlsson et al., 2011; NORCOR, 1975; Otsuka et al., 2004; Wolfe and Hoult, 1974). Most of the fluid exchange is confined to the region near the ice–water interface where the volume fraction and morphology of the pore space are challenging to quantify (e.g., Cox and Weeks, 1975; Krembs et al., 2000; Notz and Worster, 2008; Weissenberger et al., 1992). However, past field and laboratory measurements indicate that volume-averaged bulk oil entrainment is dependent on a porosity

threshold that separates ice susceptible to infiltration from that that is not susceptible (e.g. Karlsson et al., 2011; NORCOR, 1975). Based on those observations and 12 years of measurements of physical properties of landfast, first-year sea ice at Barrow, Alaska, the accessible sea ice volume and potential entrainment volume of oil are estimated in this study. The focus of this study is on growing columnar ice with a lamellar ice–ocean interface, i.e. not including granular ice or thin sea ice, or ice with protruding platelets (Jeffries et al., 1995; Petrich and Eicken, 2010). Oil infiltration into this ice type has been investigated in field and laboratory experiments used in the present study (Karlsson, 2009; Karlsson et al., 2011; NORCOR, 1975).

Modes of interaction between oil and sea ice have been reviewed by Fingas and Hollebone (2003). Oil impinging on the underside of sea ice spreads laterally as a film or as discrete droplets. The lateral extent of spread is limited by the bottom topography of sea ice, which gives rise to the concept of pooling capacity (e.g., Wilkinson et al., 2007). Once the oil is stationary, a lip of sea ice will grow over the oil lens, encapsulating and immobilizing oil. Ice above the oil lens entrains oil into the connected brine pore space, such that the oil extends

* Corresponding author.

E-mail address: christian.petrich@norut.no (C. Petrich).

through the skeletal layer (the lowermost layer exhibiting high porosities and no mechanical strength) into the ice above and into brine channels. Dickins (1992) reviewed laboratory and field studies that investigated oil entrainment in sea ice. Summaries of more recent work were provided, among others, by Buist et al. (2008) and Dickins (2011). For the purpose of this study, the most relevant and detailed data on oil entrainment in ice are those of Martin (1979) and NORCOR (1975) for field work, and Karlsson et al. (2011) and Otsuka et al. (2004) for laboratory studies.

One of the first studies investigating the fate of oil released under sea ice from winter through spring was the NORCOR experiment in landfast first-year sea ice in the Canadian Arctic (Martin, 1979; NORCOR, 1975). It demonstrated that most of the oil spilled in fall and winter was entrained as lenses pooling under and then encapsulated in the ice. In spring, as the ice started to warm, oil began to migrate upward as brine channels increased in size. Eventually, oil reached the surface through discrete channels in May. As the ice continued to deteriorate, the oil progressively saturated the interstices within and between ice crystals. Oil continued to flow upward through the ice until surface ablation had fully exposed the level of initial oil-lens entrainment. The average concentration of oil in oil-saturated sea ice was 4.5%, with a maximum of 7% in a 4 cm section.

Recently, Karlsson et al. (2011) reported on results of laboratory experiments on oil entrainment in sea ice. They grew ice to approximately 0.15 m thickness, injected oil under the ice, allowed the oil lens to become encapsulated, raised the ambient temperature in some experiments, and then determined vertical profiles of oil concentration and ice properties. Including similar measurements of Otsuka et al. (2004), they found that samples with porosity above 0.1 contained oil, and that oil concentration maintained a maximum of approximately 5% by mass for porosities above 0.15. Results did not reveal differences between the 3 different crude oils used, or dependence on warming of the ice prior to excavation. Based on this prior work, we estimate bulk oil entrainment as a constant 4.5% by mass for ice of a porosity above a threshold that we consider to vary between 0.1 and 0.15. Hence, the present study explores the question as to how much oil may be retained in columnar (i.e., congelation) sea ice as a function of the distance of this porosity threshold from the ice–ocean interface. A further motivation for this study derives from the fact that recent work by Wilkinson et al. (2007) has led to improved estimates of oil pooling under sea ice but does not consider the entrainment and immobilization of oil into the high-porosity bottom sea ice layers. A comprehensive model of oil–ice interaction such as those reviewed by Reed et al. (1999), however, requires better estimates and parameterizations of immobilization of oil in the bottom layers. Such processes are also of importance in assessing the impact of oil on sea-ice microbial communities, which are typically concentrated in the very same subvolume of the ice cover.

2. Methods

To achieve the goals of this study, field measurements of sea ice bulk salinity and temperature profiles were used to calculate porosity profiles under different boundary conditions relevant in the context of oil release under sea ice. These profiles were interpreted in the context of previous work, relating the porosity profile to potential oil entrainment. Salinity data were available for 12 years while temperature profile time series were available for only 6 years. In order to obtain temperature profiles applicable for all cores and to aid in the development of parameterization schemes we devised three temperature scenarios for each day of the year (cold, average, and warm) and determined three corresponding porosity profiles for each of the salinity cores.

Ice sampling and characterization were carried out in level landfast sea ice in the Chukchi Sea at Barrow, Alaska, between Ukpeagvik Iñupiat Corporation Naval Arctic Research Lab (UIC-NARL) and Point Barrow.

The landfast ice at this location is representative of undeformed level ice common in many of the regions targeted for offshore oil and gas development, in particular in the Chukchi and Beaufort Seas. Each year, a location approximately 0.5 to 2 km offshore near Barrow was chosen for repeat measurements. The investigated ice was level first-year ice that started to form between November and December and continued to increase in thickness until the end of May. Water depth was approximately 6 m. In general, a limited amount of snow melt took place in May and meltpond formation began in June (Petrich et al., 2012).

Sea ice cores for salinity determination were taken with a fiberglass core barrel (10 cm diameter) and immediately sectioned into vertical segments on site to minimize loss of brine from the ice (Eicken, 2010). 55 cores used in this study had a vertical sampling size at the bottom of approximately 0.05 m or less and were taken between 2000 and 2011. Of these cores, 8 cores were sampled at a vertical section thickness of 0.03 m or less.

Starting in the winter of 2005/6, an automated probe was used to record profiles of water and ice temperature in vertical intervals of 0.1 m (Druckenmiller et al., 2009). Measurements were performed at intervals of 5 to 30 min from January or February until June. In order to determine porosity profiles, the ice temperature profile is needed at the ice–water interface. We determined this profile by determining a best fit curve for adjacent thermistors as described below.

The complete set of salinity and temperature measurements is archived as part of the Seasonal Ice Zone Observing Network (SIZONet) and is available through the Advanced Cooperative Arctic Data and Information Service (ACADIS, <http://www.aoncadis.org/>; Eicken et al., 2008).

For the ice considered here, the temperature follows an approximately linear profile above the ice–water interface and is depth-independent below the ice–water interface (Petrich and Eicken, 2010). Deviations from the linear profile are most pronounced close to the ice surface where ice temperature responds quickly to air temperature variations and seasonal warming. Since this region is not of interest, the fitting algorithm was restricted to temperature data at least 0.4 m below the ice–snow interface, and no more than 1.0 m above the ice–water interface. For each temperature profile, least-square optimization was used to find the parameters T_w , z_{IF} , dT/dz , and d^2T/dz^2 of the equation

$$T(z) = \begin{cases} T_w & \text{for } z - z_{IF} < 0 \\ T_w + \frac{dT}{dz}(z - z_{IF}) + \frac{d^2T}{dz^2}(z - z_{IF})^2 & \text{for } z - z_{IF} \geq 0 \end{cases}, \quad (1)$$

where T is temperature, z is vertical position, $z - z_{IF}$ is the vertical position above the ice–water interface, T_w is the depth-independent water temperature, dT/dz is the temperature gradient above the ice–water interface ($dT/dz < 0$), and d^2T/dz^2 is the curvature of the ice temperature profile. Visual inspection showed that the second-order fit produces unrealistic results in the presence of strong temperature gradients early in the season. As a result, we performed a linear fit prior to day-of-year 65, i.e. $d^2T/dz^2 = 0$ was prescribed in Eq. (1). The time series of temperature measurements are available through ACADIS.

Temperature and salinity were used to calculate profiles of porosity, ϕ , from phase relationships given by Cox and Weeks (1983) and Leppäranta and Manninen (1988) (cf. Petrich and Eicken, 2010). An air content of 0 was assumed since the ice under consideration was below the freeboard line and we are only considering the pore space connected to seawater. Porosity profiles were calculated at 1 mm increments based on a linear temperature profile and bulk salinity measured at the corresponding depth.

Sea ice data from Barrow, Alaska, were related to oil-in-ice experiments in the Canadian Arctic and laboratory studies, all performed on structurally similar, columnar ice. Laboratory tank experiments were performed under quiescent conditions, and sea ice had a lamellar ice–ocean interface and crystal structure representative of undeformed

first-year sea ice at Barrow (Karlsson, 2009; Karlsson et al., 2011). Field experiments were performed under undeformed landfast first-year sea ice in the Canadian Arctic with seawater salinity, water depth, low tidal range (0.3 m), and ice thickness similar to conditions at Barrow (Druckemiller et al., 2009; NORCOR, 1975; Petrich et al., 2012). The “feeble” under-ice currents in the Canadian Arctic correspond to quiescent conditions in the laboratory (NORCOR, 1975). Bulk sea ice salinity was highest in laboratory experiments and lowest in the Canadian Arctic. However, since oil entrainment is expressed in relation to ice porosity, observations of field and laboratory experiments are comparable (Karlsson et al., 2011).

Accessible pore space was defined as the volume below the lowest horizon of threshold porosity φ , z_x . This threshold porosity was motivated by bounds on oil entrainment summarized by Karlsson et al. (2011). Oil entrainment was observed in ice of $\varphi > 0.10$, with saturated entrainment beginning at $\varphi > 0.15$. Hence, entrainment depth z_x was calculated for both $\varphi = 0.10$ and $\varphi = 0.15$ in order to estimate the range of likely entrainment volumes.

Because bulk salinity and porosity change appreciably over a narrow range at the ice–ocean interface (Notz and Worster, 2008), penetration depths were included in the quantitative analysis only if they exceeded the thickness of the bottom-most salinity samples. However, excluded depths are plotted for completeness.

In oil-entrained sea ice samples, crude oil has been found to occupy typically 4.5%–mass by mass of sea ice. For a typical oil density around 800 kg/m^3 this translates into entrainment of 5.5% by volume. The volume of entrained oil was therefore calculated as 5.5% of the entrainment depth z_x .

3. Results

Sea ice salinity cores extracted from the ice between 2000 and 2011 show consistency of ice thickness as evident in Fig. 1 which plots the length of all cores as a function of day of year. Ice thickness increased from approximately 0.6 m in January to 1.5 m in May. The inter-annual variability in ice thickness was approximately $\pm 0.15 \text{ m}$ for any given day of year. The consistency in ice thickness enables analysis without taking ice thickness into account explicitly. At the same time, the observed evolution of ice thickness is representative both of landfast ice and of undeformed level first-year ice that formed during fall freeze-up in the open ocean of the Chukchi and Beaufort Seas.

Temperature gradients at the ice–ocean interface were calculated from the vertical temperature profiles for 2006 to 2011. Fig. 2 shows that the temperature gradient at the interface tended to decrease in magnitude over the course of the season, which is expected due to a combination of increasing ice thickness, snow depth, and air temperatures. Three temperature scenarios at the ice–water interface were derived from these data, representing cold, average, and warm ice conditions. The cold and warm scenarios correspond to the most extreme observations in the data record, while the average scenario

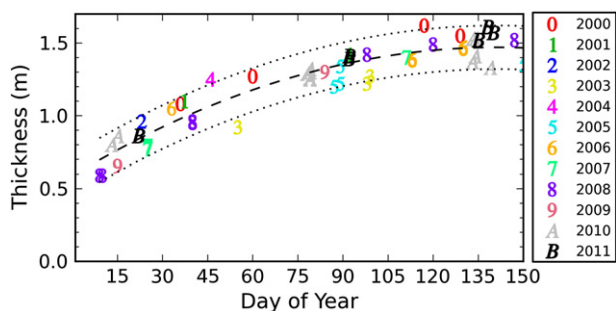


Fig. 1. Ice thickness, H , of salinity cores used in this study as a function of day-of-year (day). The dashed line follows the best fit line $H = 0.59 \text{ m} + 0.013 \text{ m } day - 4.4 \times 10^{-5} \text{ m } day^2$, the dotted lines delineate the $\pm 0.15 \text{ m}$ interval around the dashed line.

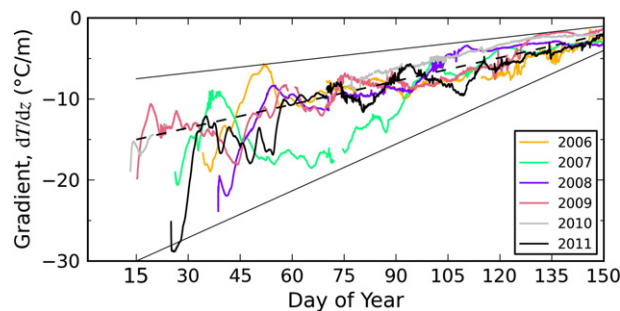


Fig. 2. Ice temperature gradients at the ice–ocean interface, dT/dz , derived from temperature probe data as a function of day-of-year. The dashed line indicates the average temperature scenario used, while the upper and lower thin solid lines indicate warm and cold scenarios, respectively.

represents the typical development of the temperature gradient. Temperature profiles of the respective scenarios were defined using

$$T(z) = T_w + \frac{dT}{dz}(z - z_{IF}), \quad (2)$$

with water temperature $T_w = -1.8 \text{ }^\circ\text{C}$. The scenario-dependent temperature gradient was defined as

$$\frac{dT}{dz} = \left(\frac{dT}{dz}\right)_{DOY=15} + \left[\left(\frac{dT}{dz}\right)_{DOY=150} - \left(\frac{dT}{dz}\right)_{DOY=15} \right] \frac{DOY - 15}{135}, \quad (3)$$

where DOY is the day of year and temperature gradients on $DOY = 15$ and 150 are listed in Table 1.

Porosity profiles were calculated based on the measured salinity profiles and representative temperature profiles of Eq. (2). A typical example profile is shown in Fig. 3. The expected depth of penetration z_x , i.e. the distance of the porosity threshold from the ice–water interface, is shown in Figs. 4 and 5 for $\varphi = 0.10$ and 0.15 , respectively. Data are scattered but a trend is discernible that shows that the penetration depth increases from January to May in all cases. Also, penetration depth increases with ice temperature. Key data derived from a linear best fit are given in Table 1. For the average temperature scenario, depth to $\varphi = 0.10$ increases from 0.04 m in mid January to 0.12 and 0.18 m at the end of March and May, respectively (Fig. 4b). For $\varphi = 0.15$, no numbers were derived for mid January because the depth is less than the thickness of the bottom-most samples in all cases. However at the end of March and May depths are half of the respective values determined for $\varphi = 0.10$ (Fig. 5b). Depending on the temperature scenario, derived depths of fluid penetration range from 0.02 to 0.10 m in January to 0.12 to 0.25 m in May for a porosity threshold of 0.10 (Fig. 4a and c).

The potential oil entrainment based on both $\varphi = 0.1$ and 0.15 is given in Table 1. Entrainment volumes increase with the season and are higher during a warm spell than during a cold spell. While entrainment during a cold spell in January is expected to be less than 1 L/m^2 , entrainment could be as high as 5 to 10 L/m^2 during a warm spell in late March. By the end of May, entrainment of 4 to 13 L/m^2 should be expected, depending on ice temperature.

4. Discussion

Calculated depths of entrainment shown in Figs. 4 and 5 scatter. This may be due to at least two factors: the way porosity was calculated and the stochastic nature of the spatial bulk salinity distribution. Scatter is expected due to the way porosity was calculated. While the temperature profile used is a continuous function with depth, the bulk salinity profile is discontinuous at the edges of the sample volumes. The resulting porosity profile reflects this step profile, introducing a vertical uncertainty of plus or minus one half of the vertical

Table 1

Temperature gradients dT/dz (Fig. 2), entrainment depths z_x , and oil content at day-of-years 15, 90, and 150, representing beginning, middle, and end of the data record, respectively. Entrainment depths are given for porosity thresholds 0.1 (Fig. 4) and 0.15 (Fig. 5). Oil content is calculated from entrainment depths assuming 5.5% entrainment by volume and $\phi=0.15$ (values for $\phi=0.1$ are given in brackets).

Scenario	Cold			Average			Warm		
	15	90	150	15	90	150	15	90	150
dT/dz ($^{\circ}\text{C}/\text{m}$)	-30	-16	-4	-15	-8	-2	-7.5	-4	-1
z_x (m), $\phi=0.10$	0.02	0.08	0.12	0.04	0.12	0.18	0.10	0.18	0.25
z_x (m), $\phi=0.15$		0.04	0.07		0.06	0.09		0.08	0.10
Oil (L/m^2)	(1)	2 (4)	4 (7)	(2)	3 (7)	5 (10)	(5)	4 (10)	5 (13)

sample size (i.e., ± 0.025 m in most cases). However, this effect cannot explain the range of scatter observed toward May.

Scatter is also to be expected on physical grounds as each data point is derived from a single salinity core and salinity core data are known to contain a stochastic component (e.g. Bennington, 1967; Gough et al., 2012). For example, Gough et al. (2012) found that salinity between cores must differ by at least 29% for them to be considered different with 90% confidence. This can be converted into an estimate of the expected scatter in depth z_x for Fig. 4b (i.e., z_x based on $\phi=0.10$ for average ice temperatures) from the relationship between bulk salinity, porosity and temperature: in linear approximation, the phase relationship takes on the form

$$\phi \propto \frac{S}{T_w + \frac{dT}{dz}(z - z_{IF})} \quad (4)$$

where S is the bulk sea ice salinity. For any particular porosity ϕ , an uncertainty in S of $\pm 14.5\%$ (i.e., the window of 29% given by Gough et al., 2012) is equivalent to a temperature range of $\pm 14.5\%$. At a temperature of -2.5 $^{\circ}\text{C}$ (e.g., $\phi=0.10$ if $S=5$), this temperature range of ± 0.36 $^{\circ}\text{C}$ corresponds to an uncertainty of the vertical position z of ± 0.024 and ± 0.18 m for $dT/dz = -15$ and -2 $^{\circ}\text{C}/\text{m}$, respectively. Hence, scatter expected around the best fit line in Fig. 4b is ± 0.024 m and ± 0.18 m in mid January and late May, respectively. The range spanned by data in Fig. 4b is actually smaller than this (± 0.02 and ± 0.10 m, respectively), supporting the conclusion that the scatter observed is consistent with expectations due to natural variability of sea ice bulk salinity.

Brine loss from the bottom-most layers of sea ice may impact measured salinities and hence derived porosities. As shown by Notz and Worster (2008), in thin young ice, as much as the bottom 5 cm

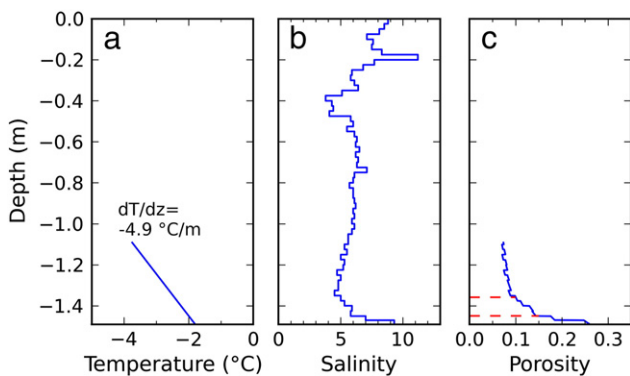


Fig. 3. Example of (a) temperature, (b) salinity and (c) porosity profiles under the average temperature scenario applied to salinity data of 29 April 2008. Temperature and porosity were calculated for the bottom-most 0.4 m. The dashed lines in (c) mark the depths of porosity 0.10 and 0.15, respectively.

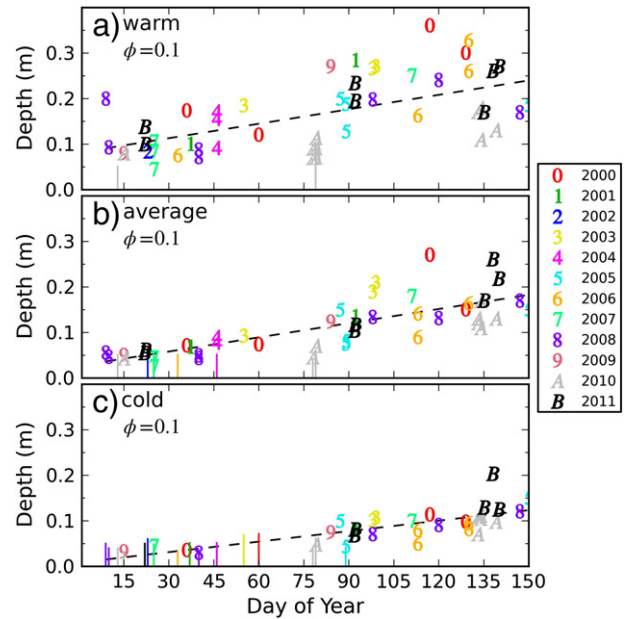


Fig. 4. Oil penetration depth based on porosity threshold $\phi=0.1$ for temperature scenarios (a) warm, (b) average, and (c) cold. The length of vertical lines indicates penetration depths within the bottom-most salinity sample that were excluded from the quantitative analysis. The dashed best fit lines indicate the general trend of the respective scenarios.

may greatly exceed porosities of 0.1 to 0.2, with near-constant lower porosities above this bottom layer. For thicker ice (>0.1 m) the high porosity of the bottom-most few cm appears to result in a substantial underestimation of the bulk salinity and hence brine volume fraction, even for rapid on site sampling as practiced here. While the determination of the location of the 0.1 or 0.15 porosity horizons for thicker ice is less impacted by such brine loss, brine loss during sampling would result in a slight underestimate of entrainment depth and hence underestimate of oil entrainment. At the same time, since simultaneous measurements of ice salinity and oil content in high

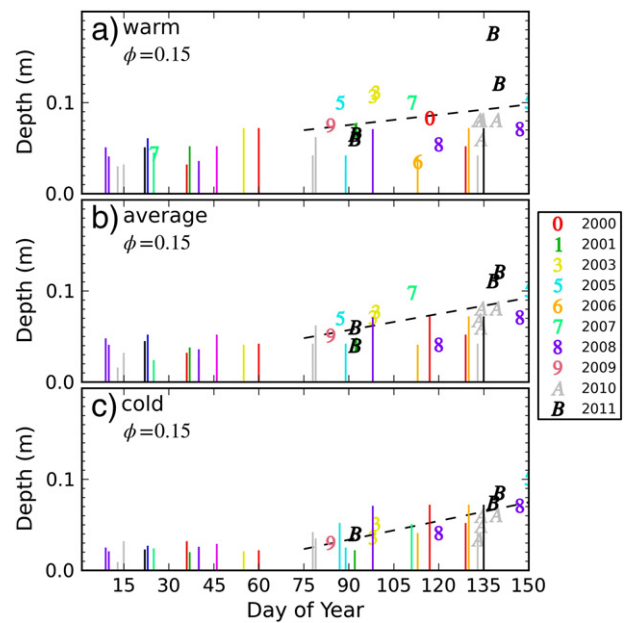


Fig. 5. Oil penetration depth based on porosity threshold $\phi=0.15$ for temperature scenarios (a) warm, (b) average, and (c) cold. The length of vertical lines indicates penetration depths within the bottom-most salinity sample that were excluded from the quantitative analysis. The dashed best fit lines indicate the general trend of the respective scenarios.

porosity regions ($\phi > 0.3$) are not available, the initial assumption of porosity-independence of oil content could be violated. In this case, the volume fraction of oil entrained into sea ice will likely be underestimated. For example, if we assume as an upper limit an oil volume fraction of 30% in the bottom-most 3 to 10 mm of sea ice, this effect might increase the amount of oil entrained per square meter by up to 1–3 L.

A distinction should be emphasized between the influence of warm and cold spells and years with systematically above- or below-normal ice temperatures. Bulk salinity depends on the temperature profile at the time of ice formation in a way that higher temperatures generally lead to the formation of less saline ice (e.g. Kovacs, 1996; Petrich et al., 2006, 2011). Hence, while brief warm periods increase porosity temporarily (Eq. (4)), extended warm periods decrease interface porosity resulting in the formation of low-salinity ice. This is illustrated by data of 2010, which experienced comparatively high ice temperatures (Fig. 2), resulting in slower growth rates and lower bulk salinity (not shown). The lower bulk salinity is reflected in Figs. 4 and 5 as smaller entrainment depths from March onward, in spite of generally warm ice temperatures. The net effect of this feedback is that entrainment depth z_x may be unseasonally large in ice warming up after having grown under colder-than-average conditions. Anomalies in the snow cover at the site of interest can have a comparable impact, such that deeper-than-normal snow cover will tend to decrease ice growth rates and hence salinities over the course of the season. For ice types with substantially different roughness, such as ridged or rubble ice, locally variable snow depth may result in spatially variable oil entrainment potential.

Entrainment of oil in the interstitial space of the ice matrix can be expected to contribute to the oil pooling capacity of warm ice. Two methods have been used to estimate the expected pooling of oil in under-ice depressions (Wilkinson et al., 2007). Traditionally, only statistical information on ice topography has been used to assess pooling potential. Following the statistical method, oil pooling is assumed to take place in all pronounced depressions, and capacity has been estimated to average at 30 L/m² (Wilkinson et al., 2007). However, more recent calculations based on actual under-ice topography and a gravity flow model suggested that pooling may only result in retention of 4 L/m² (Wilkinson et al., 2007). In the gravity flow model, oil is distributed assuming the absence of currents (consistent with field and laboratory experiments used in this study), while the oil distribution mechanism is undefined in the statistical model. Oil entrainment in the interstitial space of the ice matrix adds to the pooling capacity. For the case of landfast ice at Barrow, Alaska, it was found that entrainment volumes of 10 L/m² may be observed in warm ice. These entrainment volumes are valid for ice that is homogeneously oil-covered over a hitherto unspecified period required for entrainment (the time scale is likely to be of the order of hours or days; NORCOR, 1975). Based on the two different methods mentioned above, 50% and 9% of the ice underside are expected to be oil-covered, respectively (Wilkinson et al., 2007). Hence, the effective entrainment averaged over a large scale would also be reduced to 50% or 9% of the values given in Table 1, respectively. Based on 10 L/m² entrainment in warm ice, an areal coverage of 50% and 9% for the statistical estimate and the gravity model, would contribute an additional 15% and 25%, respectively, to the oil retention capacity under ice.

5. Conclusion

Based on a 12-year record of salinity data and 6 years of ice temperature data at Barrow, Alaska, we find that the potential volume of oil entrained in the interstitial space of the sea ice crystal fabric increases from January to May. Entrainment may reach approximately 20% of the potential oil volume pooled beneath sea ice, with the latter based on estimates by Wilkinson et al. (2007). Analyses for different regions could be performed based on available sea ice salinity and

ice temperature data. Further, entrainment depths determined in this study would be relevant beyond the scope of oil entrainment, for example in the context of habitat available for ice biota.

In the context of oil-spill impact assessment it will be valuable to assess the mechanism and rate of oil entrainment as there is no evidence that oil, once entrained in the ice continues to spread laterally (Martin, 1979; NORCOR, 1975). Further, two mechanisms related to the presented work could lead to a drastic increase of the entrainment potential. These are vertical migration of oil through the ice leading to release at the surface at the end of May (Karlsson et al., 2011; NORCOR, 1975), and the formation of Arctic platelet ice due to meltwater beneath sea ice (Jeffries et al., 1995). As shown by Eicken (1994), such ice formation is particularly prominent in bottom ice surface depressions and hence likely to trap and potentially greatly increase the entrainment potential for oil. A quantitative assessment and modeling of these processes would improve and could potentially alter response to oil spills. The results of this study indicate that oil entrainment in the interstitial space between ice crystals contributes to oil spatial fixation and temporary removal from the oceans.

Acknowledgments

This work was funded by the Norwegian Research Council, project number 195160, and Eni Norge. Data at Barrow, Alaska, were acquired under research grants OPP-0632398 and OPP-0856867, with additional support from grant OPP-0934683, of the National Science Foundation, USA. The constructive comments of two anonymous reviewers are gratefully acknowledged.

References

- Bennington, K.O., 1967. Desalination features in natural sea ice. *Journal of Glaciology* 6 (48), 845–857.
- Buist, I., Belore, R., Dickins, D., Hackenberg, D., Guarino, A., Wang, Z., 2008. Empirical Weathering Properties of Oil in Ice and Snow. Final Report. Project Number 1435-01-04-RP-34501. U.S. Department of the Interior Minerals Management Service, Anchorage, Alaska, USA. (170 pp.).
- Cota, G.F., Smith, R.E.H., 1991. Ecology of bottom ice algae: II. Dynamics, distributions and productivity. *Journal of Marine Systems* 2, 279–295.
- Cox, G.F.N., Weeks, W.F., 1975. Brine Drainage and Initial Salt Entrapment in Sodium Chloride Ice, Research Report 345. Cold Regions Research and Engineering Lab, Hanover, NH, USA. (88 pp.).
- Cox, G.F.N., Weeks, W.F., 1983. Equations for determining the gas and brine volumes in sea-ice samples. *Journal of Glaciology* 29 (102), 306–316.
- Dickins, D.F., 1992. Behavior of Spilled Oil at Sea (BOSS): Oil-in-Ice Fate and Behavior. Environment Canada, U.S. Minerals Management Service, and American Petroleum Institute. (342 pp.).
- Dickins, D.F., 2011. Behavior of oil spills in ice and implications for Arctic spill response. Proceedings of the OTC Arctic Technology Conference, 7–9 February 2011, Houston, Texas, USA, OTC 22126, pp. 1–15.
- Druckenmiller, M.L., Eicken, H., Johnson, M.A., Pringle, D.J., Williams, C.C., 2009. Toward an integrated coastal sea-ice observatory: system components and a case study at Barrow, Alaska. *Cold Regions Science and Technology* 56, 61–72.
- Eicken, H., 1994. Structure of under-ice melt ponds in the central Arctic and their effect on the sea-ice cover. *Limnology and Oceanography* 39 (3), 682–694.
- Eicken, H., 2010. Ice sampling and basic sea ice core analysis. In: Eicken, H., et al. (Ed.), *Field Techniques for Sea Ice Research*. University of Alaska Press, pp. 117–140.
- Eicken, H., Gradinger, R., Kaufman, M., Petrich, C., 2008. Sea-ice core measurements (SIZONET). Dataset 26 August 2008, updated 2012. UCAR/NCAR – CISL – ACADIS. <http://dx.doi.org/10.5065/D63X84KG>.
- Eide, L., Martin, S., 1975. The formation of brine drainage features in young sea ice. *Journal of Glaciology* 14, 137–154.
- Fingas, M.F., Hollebone, B.P., 2003. Review of behavior of oil in freezing environments. *Marine Pollution Bulletin* 47, 333–340.
- Gough, A.J., Mahoney, A.R., Langhorne, P.J., Williams, M.J.M., Haskell, T.G., 2012. Sea ice salinity and structure: a winter time series of salinity and its distribution. *Journal of Geophysical Research* 117, C03008. <http://dx.doi.org/10.1029/2011JC007527>.
- Gradinger, R.R., Kaufman, M.R., Bluhm, B.A., 2009. Pivotal role of sea ice sediments in the seasonal development of near-shore Arctic fast ice biota. *Marine Ecology Progress Series* 394, 49–63.
- Jeffries, M.O., Schwartz, K., Morris, K., Veazey, A.D., Krouse, H.R., Gushing, S., 1995. Evidence for platelet ice accretion in Arctic sea ice development. *Journal of Geophysical Research* 100 (C6), 10,905–10,914. <http://dx.doi.org/10.1029/95JC00804>.
- Karlsson, J., 2009. Oil movement in sea ice. Masters Thesis, University of Copenhagen, Copenhagen, Denmark, 199 pp.
- Karlsson, J., Petrich, C., Eicken, H., 2011. Oil entrainment and migration in laboratory-grown saltwater ice. Proceedings of the 21st International Conference on Port and

- Ocean Engineering under Arctic Conditions 10–14 July 2011, Montréal, Canada. POAC11-186, pp. 1–10.
- Kovacs, A., 1996. Sea Ice: Part I. Bulk salinity versus ice floe thickness. Report 96-7. Cold Regions Research and Engineering Laboratory, Hanover, NH, USA. (23 pp.).
- Krembs, C., Gradinger, R., Spindler, M., 2000. Implications of brine channel geometry and surface area for the interaction of sympagic organisms in Arctic sea ice. *Journal of Experimental Marine Biology and Ecology* 243, 55–80.
- Leppäranta, M., Manninen, T., 1988. The brine and gas content of sea ice with attention to low salinities and high temperatures. Finnish Institute of Marine Research Internal Report 1988, 2 (15 pp.).
- Martin, S., 1979. A field study of brine drainage and oil entrainment in first-year sea ice. *Journal of Glaciology* 22, 473–502.
- NORCOR, 1975. The interaction of crude oil with Arctic sea ice. Beaufort Sea Technical Report, 27. Department of the Environment, Canada (213 pp.).
- Notz, D., Worster, M.G., 2008. In situ measurements of the evolution of young sea ice. *Journal of Geophysical Research* 113 (C03001), 1–7. <http://dx.doi.org/10.1029/2007JC004333>.
- Otsuka, N., Kondo, H., Saeki, H., 2004. Experimental study on the characteristics of oil ice sandwich. Proceedings of OCEANS '04 MTS/IEEE–TECHNO-OCEAN '04., vol. 3, 9–12 Nov. 2004, Kobe, Japan, pp. 1470–1475.
- Petrich, C., Eicken, H., 2010. Growth, structure, and properties of sea ice, In: Thomas, D.N., Dieckmann, G.S. (Eds.), *Sea Ice*, 2nd ed. Wiley-Blackwell, pp. 23–77.
- Petrich, C., Langhorne, P.J., Sun, Z.F., 2006. Modelling the interrelationships between permeability, effective porosity and total porosity in sea ice. *Cold Regions Science and Technology* 44 (2), 131–144. <http://dx.doi.org/10.1016/j.coldregions.2005.10.001>.
- Petrich, C., Langhorne, P., Eicken, H., 2011. Modelled bulk salinity of growing first-year sea ice and implications for ice properties in spring. Proceedings of the 21st International Conference on Port and Ocean Engineering under Arctic Conditions 10–14 July 2011, Montréal, Canada. POAC11-187, pp. 1–10.
- Petrich, C., Eicken, H., Zhang, J., Krieger, J.R., Fukamachi, Y., Ohshima, K.I., 2012. Coastal sea ice melt and break-up in northern Alaska: processes and possibility to forecast. *Journal of Geophysical Research* 117 (C02003), 1–19. <http://dx.doi.org/10.1029/2011JC007339>.
- Reed, M., Johansen, O., Brandvik, P.J., Daling, P., Lewis, A., Fiocco, R., Mackay, D., Prentki, R., 1999. Oil spill modeling towards the close of the 20th century: overview of the state of the art. *Spill Science & Technology Bulletin* 5 (1), 3–16.
- Weissenberger, J., Dieckmann, G., Gradinger, R., Spindler, M., 1992. Sea ice: a cast technique to examine and analyze brine pockets and channel structure. *Limnology and Oceanography* 37 (1), 179–183.
- Wilkinson, J.P., Wadhams, P., Hughes, N.E., 2007. Modelling the spread of oil under fast sea ice using three-dimensional multibeam sonar data. *Geophysical Research Letters* 34, L22506. <http://dx.doi.org/10.1029/2007GL031754>.
- Wolfe, L.S., Houlst, D.P., 1974. Effects of oil under sea ice. *Journal of Glaciology* 13 (69), 473–488.